Based on the aforementioned results, it may be concluded that both the present method and the method of Green[5] provide adequate predictions of the development of turbulent, compressible boundary layers on adiabatic walls for the range of experimental conditions considered in Refs. 13 and 16–19. However, the present method has been shown to give an improvement in accuracy, relies less on empiricism and represents a simpler and more direct extension of Head's[1] incompressible entrainment theory to compressible flows.

References

[1] Head, M. R., "Entrainment in the Turbulent Boundary Layer," R and M 3152, 1958, Aeronautical Research Council, London.

[2] Cumpsty, N. A. and Head, M. R., "The Calculation of Three-Dimensional Turbulent Boundary Layers Part I: Flow Over the Rear of an Infinite Swept Wing," *Aeronautical Quarterly*, Vol. 18, 1967, pp. 55–84.

[3] Standen, N. M., "A Concept of Mass Entrainment Applied to Compressible Turbulent Boundary Layers in Adverse Pressure Gradients," *Proceedings of the 4th Congress of the International Council of the Aeronautical Sciences*, Spartan Books, London, 1965, pp. 1101–1125.

[4] So, R. M. C., "An Extension of a Turbulent Incompressible Boundary Layer Theory to Compressible Boundary Layers," TN 65-6, 1965, McGill University, Montreal, Canada.

[5] Green, J. E., "The Prediction of Turbulent Boundary Layer Development in Compressible Flow," *Journal of Fluid Mechanics*, Vol. 31, 1968, pp. 753–778.

[6] Der, J. J., "Theoretical Study of the Separation of Subcritical and Supercritical Turbulent Boundary Layers by the Method of Integral Equations," AIAA Paper 69-34, New York, 1969.

[7] Dvorak, F. A., "Calculation of Turbulent Boundary Layers on Rough Surfaces in Pressure Gradient," *AIAA Journal*, Vol. 7, No. 9, Sept. 1969, pp. 1752–1759.

[8] Cham, T-S. and Head, M. R., "Turbulent Boundary Layer Flow on a Rotating Disk," *Journal of Fluid Mechanics*, Vol. 37, 1969, pp. 129–147.

[9] Cham, T-S. and Head, M. R., "The Turbulent Boundary Layer on a Rotating Cylinder in an Axial Stream," *Journal of Fluid Mechanics*, Vol. 42, 1970, pp. 1–15.

[10] Alber, I. E. and Coats, D. E., "Analytical Investigations of Equilibrium and Nonequilibrium Compressible Turbulent Boundary Layers," AIAA Paper 69-689, San Francisco, Calif., 1969.

[11] McDonald, H., "An Assessment of Certain Procedures for Computing the Compressible Turbulent Boundary Layer Development," *Compressible Turbulent Boundary Layers*, NASA SP-216, 1968, pp. 181–229.

[12] Sasman, P. K. and Cresci, R. J., "Compressible Turbulent Boundary Layer with Pressure Gradient and Heat Transfer," *AIAA Journal*, Vol. 4, No. 1, Jan. 1966, pp. 19–25.

[13] Winter, K. G., Smith, K. G., and Rotta, J. C., "Turbulent Boundary Layer Studies on a Waisted Body of Revolution in Subsonic and Supersonic Flow," AGARDograph 97, Pt. II, May 1965, pp. 933–961.

[14] Spence, D. A., "The Growth of Compressible Turbulent Boundary Layers on Isothermal and Adiabatic Walls," R and M 3191, 1961, Aeronautical Research Council, London.

[15] Eckert, E. R. G., "Engineering Relations for Friction and Heat Transfer to Surfaces in High Velocity Flow," *Journal of the Aeronautical Sciences*, Vol. 22, 1955, pp. 585–587.

[16] Winter, K. G., Smith, K. G., and Gaudet, L., "Measurements of Turbulent Skin Friction at High Reynolds Numbers at Mach Numbers of 0.2 and 2.2," AGARDograph 97, Pt. I, May 1965, pp. 97–124.

[17] Matting, F. W. et al., "Turbulent Skin Friction at High Mach Numbers and Reynolds Numbers in Air and Helium," TR R-82, 1961, NASA.

[18] Korkegi, R. H., "Transition Studies and Skin-Friction Measurements on an Insulated Plate at a Mach Number of 5.8," *Journal of the Aeronautical Sciences*, Vol. 23, 1956, pp. 97–107.

[19] Pasiuk, L., Hastings, S. M., and Chatham, R., "Experimental Reynolds Analogy Factor for a Compressible Turbulent Boundary Layer with a Pressure Gradient," NOLTR 64-200, 1965, United States Naval Ordnance Lab., White Oak, Md.

Impulse of a Ring with Nonlinear Material Behavior

JOEL SWEET*
Sandia Laboratories, Livermore, Calif.

Introduction

THE linear dynamic response of nonaxisymmetric cylindrical shells has been considered to some detail in the literature. Payton[1] analyzed the impulsive membrane motion of a cylindrical shell and obtained a wave form of solution rather than the usual modal solution. The more general bending equations have been examined by Humphreys and Winter[2] using the modal technique.

The nonlinear dynamic analysis of shells and rings has almost exclusively concerned large displacements with linear stress-strain functions. Examples of analyses using nonlinear strain-displacement relationships may be found in Roth and Klosner[3] and Dowell.[4] In both of these studies, the nonlinear partial differential equations are reduced to nonlinear ordinary differential equations, using the Galerkin-Ritz technique. The analysis of perfectly plastic rate sensitive rings can be found in Perrone.[5] In his paper, Perrone obtains good correlation between approximate and numerical solutions.

The present Note considers the dynamic response of a ring whose stress-strain law is nonlinear and subject to a linear strain-displacement relationship. The results will, in general, be valid only for the first half cycle of motion. The initial conditions of the ring can be functions of the angular variable.

Equilibrium Equations and Problem Formulation

The geometric configuration is a thin walled ring of radius a, density ρ, and thickness h. For small displacements, the equilibrium equations describing membrane motion may be combined into a single equation relating hoop stress and hoop strain. This equation has been presented by Payton and is given by

$$(\partial^2\sigma/\partial\theta^2) - \sigma - \rho a^2(\partial^2\epsilon_\theta/\partial t^2) = 0 \tag{1}$$

where σ is the hoop stress, ϵ_θ is the hoop strain, θ is the angular coordinate, and t is time. The ring is assumed to be fabricated from a work hardening material whose stress-strain relationship obeys the following nonlinear equation:

$$\sigma = E(\epsilon_\theta - b\epsilon_\theta^3) \tag{2}$$

The constant E is analogous to Young's modulus, and b is a nondimensional positive constant. This relationship is valid until the absolute value of ϵ_θ is greater than $\bar{\epsilon}$; where $\bar{\epsilon}$ is the point of zero slope given by $\bar{\epsilon} = 1/(3b)^{1/2}$. The behavior of Eq. (2) is typical of a uniaxial tensile test during the loading phase. Whereas some substances (polymers for example) also obey this equation while unloading, most structural materials observe a linear stress-strain behavior during the unloading cycle. Thus, the total transient motion of the ring becomes a bookkeeping chore with different stress-strain behaviors. This study will be concerned primarily with the initial loading cycle and expressions developed will, in general, be valid only during this loading phase.

Eliminating σ from Eqs. (1) and (2), introducing the new variable ϵ, and defining the nondimensional time τ yields

$$(\partial^2\epsilon/\partial\theta^2) - \epsilon - (\partial^2\epsilon/\partial\tau^2) + \tfrac{1}{12}\{\epsilon^3 - [\partial^2(\epsilon^3)/\partial\theta^2]\} = 0 \tag{3}$$

where $\tau = t(E/\rho)^{1/2}/a$ and $\epsilon = 2\epsilon_\theta/\bar{\epsilon}$. The variable ϵ appear-

Received June 19, 1970; revision received November 4, 1970. This work was supported by the United States Atomic Energy Commission.

* Staff Member, Analytical Mechanics Division.

ing in Eq. (3) is the hoop strain normalized by $\bar{\epsilon}/2$. The Galerkin-Ritz technique will now be used to reduce Eq. (3) to a system of ordinary differential equations. A solution to Eq. (3) is assumed to be of the following form:

$$\epsilon(\theta, \tau) = \sum_{i=0} x_i(\tau) \cos i\theta \tag{4}$$

i.e., motion symmetric about $\theta = 0$. Substituting Eq. (4) into Eq. (3) results in

$$\sum_{i=0} A_i \cos i\theta = 0$$

where A_i are functions of the x_j's. Using the Galerkin-Ritz technique, there results

$$A_i = 0; \qquad i = 0, 1, 2, \ldots \tag{5}$$

If expansion (4) is limited to n terms, Eq. (5) represents n second-order nonlinear ordinary differential equations. These equations assume the following form:

$$\ddot{x}_i + (1 + i^2)x_i = (1 + i^2)C\left[\tfrac{3}{2}x_i^3 + \tfrac{1}{2}x_{i/3}^3 + 3x_i \sum_{j\neq i} x_j^2 + \tfrac{3}{2}\sum_{j\neq k} x_j^2 x_k + 3\sum_{n>m>l} x_l x_m x_n\right] \tag{6}$$

where dots denote derivatives with respect to τ, C is equal to $\frac{1}{24}$, and i varies from 0 to n. The first summation on the right-hand side of Eq. (6) is for all j except $j = i$; the second summation is for $j \neq k$, subject to the restrictions $2j + k = i$ or $|2j - k| = i$; and the third summation is for $n > m > l$ and subject to the four restrictions $l + m + n = i$, $|l - m - n| = i$, $|l + m - n| = i$, or $|l - m + n| = i$. Equation (6) may be written,

$$\ddot{x}_i + \omega_i^2 x_i = Cf_i(x_j); \qquad i = 0, 1, 2, \ldots \tag{7}$$

where ω_i^2 equals $1 + i^2$ and f_i are nonlinear functions of the n variables x_j. The next step in the problem formulation is to reduce Eq. (7) to a set of linear differential equations.

An approximate solution to Eq. (7) will be obtained using a Poincaré type of expansion. The dependent variables x_j are expanded in the following manner:

$$x_i = \sum_{j=0} x_{ij} C^j \tag{8}$$

This technique, of course, leads to unstable secular terms (internal resonance) appearing in the solution. As is elucidated in Cunningham,[6] these terms are eliminated by also expanding the ω_i. This expansion becomes

$$\omega_i^2 = \sum_{j=0} \omega_{ij}^2 C^j \tag{9}$$

The ω_{ij} are found by using Eq. (9) and by eliminating the coefficients of the resonant terms appearing in the higher order x_{ij} differential equations. Expansion (9) is actually a specialization of the Lighthill independent variable expansion described by Tsien.[7] Substituting Eqs. (8) and (9) into Eq. (7) and equating coefficients of C^j yields the x_{ij} differential equations. For $j = 0$ and $j = 1$ these equations become

$$\ddot{x}_{i0} + \omega_{i0}^2 x_{i0} = 0 \tag{10a}$$

$$\ddot{x}_{i1} + \omega_{i0}^2 x_{i1} = -\omega_{i1}^2 x_{i0} + f_i(x_{j0}) \tag{10b}$$

Higher order equations are easily obtained but cannot be written as concisely as Eq. (10).

Half-Cosine Impulse

The initial conditions for this example are given by

$$\epsilon(0,\theta) = 0 \tag{11a}$$

$$(\partial\epsilon/\partial\tau)(0,\theta) = v_0 \cos\theta; \, |\theta| < \pi/2 \tag{11b}$$

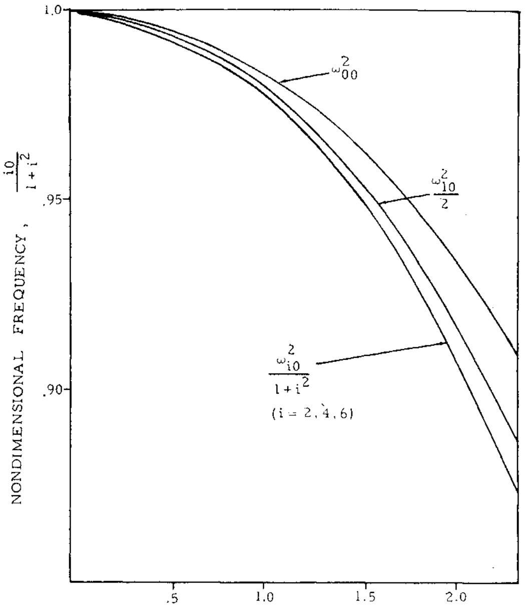

Fig. 1 Frequency-impulse amplitude relationship.

$$(\partial\epsilon/\partial\tau)(0,\theta) = 0; \, |\theta| > \pi/2 \tag{11c}$$

where v_0 may be thought of as a nondimensional strain rate and is the only parameter of the impulsive response. The initial condition concerning an impulse is often characterized by the radial impulse per area I. The relationship between v_0 and I is given by

$$v_0 = 2I(3b)^{1/2}/\rho h(\rho/E)^{1/2} \tag{12}$$

The x_{ij} initial conditions follow from Eqs. (4), (8), and (11). They are

$$x_{ij}(0) = 0 \tag{13a}$$

$$\dot{x}_{i0}(0) = u_i \tag{13b}$$

$$\dot{x}_{ij}(0) = 0; \qquad j > 0 \tag{13c}$$

where the u_i are given by

$$u_0 = v_0/\pi, \; u_1 = v_0/2$$

$$u_i = (-1)^{i/2+1} 2v_0/\pi(i^2 - 1); \qquad i = 2,4,6,8, \ldots$$

$$u_i = 0; \qquad i = 3,5,7, \ldots$$

Seven terms in Eq. (4) and two terms in Eqs. (8) and (9) have been found by the author to be sufficiently accurate (within 5%) to describe the motion indicated by Eq. (11).

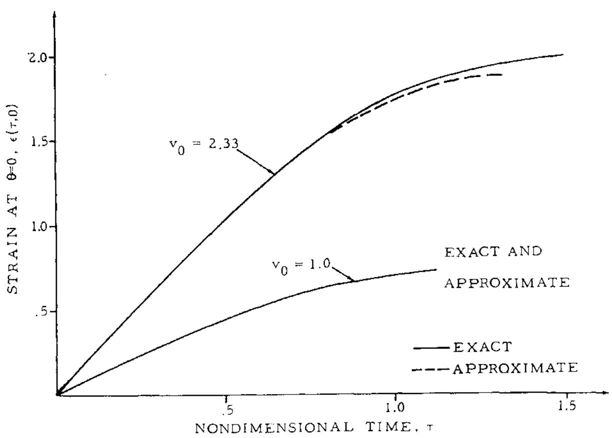

Fig. 2 Comparison of the approximate transient solution at $\theta = 0$ with the exact solution.

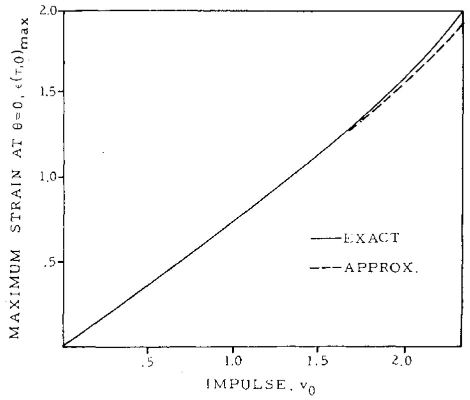

Fig. 3 Comparison of the approximate solution for the maximum strain at $\theta = 0$ with the exact solution.

The pertinent x_{i0} follow from Eqs. (10) and (13). These functions become

$$x_{i0} = (u_i/\omega_{i0}) \sin\omega_{i0}\tau \quad (14)$$

The x_{i1} differential equations are determined from Eqs. (6) and (10) and can be found in Sweet.[8] The ω_{ij} appearing in these equations must be chosen so as to eliminate the secular terms. As is demonstrated in Sweet, the elimination of the secular terms requires

$$\omega_{01}^2 = \tfrac{3}{2} \sum_{i=0} u_i^2/\omega_{i0}^2 \quad (15a)$$

$$\omega_{i1}^2 = \tfrac{3}{2}(1 + i^2)[(u_0^2/\omega_{00}^2) + \tfrac{2}{3}\omega_{01}^2 - \tfrac{1}{4}(u_i^2/\omega_{i0}^2)] \quad i = 1,2,4,6 \quad (15b)$$

$$\omega_{30}^2 = \omega_3^2 \equiv 10 \quad (15c)$$

$$\omega_{50}^2 = \omega_5^2 \equiv 26 \quad (15d)$$

The ω_{ij} can therefore be found from Eqs. (15) and the following equations:

$$\omega_i^2 = \omega_{i0}^2 + C\omega_{i1}^2; \qquad i = 0,1,2,4,6 \quad (16)$$

Equations (4, 8, 10, and 14) yield the solution for $\epsilon(\tau,\theta)$. This solution may be written as

$$\epsilon(\tau,\theta) = \sum_{i=0} \left\{ \frac{u_i}{\omega_{i0}} \sin\omega_{i0}\tau + \frac{1}{\omega_{i0}} \int_0^\tau \sin\omega_{i0}(\tau - \xi)[-\omega_{i1}^2 x_{i0} + f_i(x_{j0})]d\xi \right\} \cos i\theta \quad (17)$$

where all of the x_{k0} appearing in Eq. (17) are functions of the dummy variable ξ, the $f_i(x_{j0})$ can be found from Eqs. (6) and (10), and the ω_{ij} are given by Eqs. (15) and (16).

The impulsive response of the ring $\epsilon(\tau,\theta)$ subject to the half-cosine loading varies only with the parameter v_0. The parameter v_0, in turn, is related to the physical parameters of the ring by Eq. (12) and the normalized strain ϵ is related to the physical strain ϵ_θ by $\epsilon = 2(3b)^{1/2}\epsilon_\theta$.

The behavior of the system as a function of v_0 is presented in Figs. 1–3. The amplitude-frequency coupling typical of nonlinear systems is indicated in Fig. 1. The comparison of the approximate solution given by Eq. (17) to the finite difference solution of Eq. (3) at $\theta = 0$ appears in Figs. 2 and 3. The responses in Fig. 2 for $v_0 = 2.33$ and $v_0 = 1.0$ are plotted only up to the time when unloading occurs, since the stress-strain function of most materials changes during unloading. The maximum value of v_0 was chosen to be 2.33 because this value corresponds to a maximum hoop strain (ϵ_1) equal to $\bar{\epsilon}$. This value, of course, is the limiting value of Eq. (2). The maximum values of $\epsilon(\tau,\theta)$ at $\theta = 0$ vs v_0 are given in Fig. 3. It can be seen that the solution given by Eq. (17) agrees quite well with the exact solution for the maximum strain.

The method of solution developed in this study is not limited to a cubic stress-strain relationship, to the membrane equations, or to a half-cosine impulse. It can be extended to other stress-strain curves, to the more general bending equations, or to different initial conditions. This solution can also be combined with a linear analysis in order to analyze the behavior of a material behaving linearly during unloading. However, for most studies, the maximum strain appearing in Fig. 3 is all that is required.

References

[1] Payton, R. G., "Dynamic Membrane Stresses in a Circular Elastic Shell," *Journal of Applied Mechanics*, Vol. 83, Sept. 1961, pp. 417–420.

[2] Humphreys, J. S. and Winter, R., "Dynamic Response of a Cylinder to a Side Pressure Pulse," *AIAA Journal*, Vol. 3, No. 1, Jan. 1965, pp. 27–32.

[3] Roth, R. S. and Klosner, J. M., "Nonlinear Response of Cylindrical Shells Subjected to Dynamic Axial Loads," *AIAA Journal*, Vol. 2, No. 10, Oct. 1964, pp. 1788–1794.

[4] Dowell, E. H., "On the Nonlinear Flexural Vibrations of Rings," *AIAA Journal*, Vol. 5, No. 8, Aug. 1967, pp. 1508–1509.

[5] Perrone, N., "Impulsively Loaded Strain Hardened Rate-Sensitive Rings and Tubes," *International Journal of Solids and Structures*, Vol. 6, No. 8, Aug. 1970, pp. 1119–1132.

[6] Cunningham, W. J., *Introduction to Nonlinear Analysis*, McGraw-Hill, New York, 1958, pp. 129–130.

[7] Tsien, H. S., "The Poincaré-Lighthill-Kuo Method," *Advances in Applied Mechanics*, Vol. IV, 1956, p. 281.

[8] Sweet, J., "Dynamic Response of a Work Hardening Ring," SCL-DC-70-61, May 1970, Sandia Laboratories, Livermore, Calif.

Correlation of Inviscid Air Nonequilibrium Shock Layer Properties

Clarence J. Harris*

General Electric Company, Valley Forge, Pa.

Entropy Correlation-Analog

WITHIN an appropriate flight regime, an entropy correlation and a nozzle-shock layer analog may be combined to predict the frozen nonequilibrium properties in the inviscid inner shock layer stream tube for slender, slightly blunted, conical bodies. Early analytical work on flow expansions

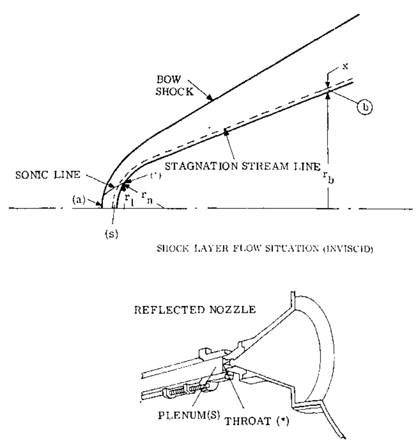

Fig. 1 Nozzle flow—shock layer analog.

Presented as Paper 70-866 at the AIAA 5th Thermophysics Conference, Los Angeles, Calif., June 29–July 1, 1970; submitted July 29, 1970; revision received November 10, 1970.

* Staff Scientist, Environmental Sciences Laboratory, RESD.